Brain-Shift: Unsupervised Pseudo-Healthy Brain Synthesis for Novel Biomarker Extraction in Chronic Subdural Hematoma

Baris Imre[1], Elina Thibeau-Sutre[1], Jorieke Reimer[3], Kuan Kho[2,3], Jelmer M. Wolterink[1]

[1] Department of Applied Mathematics, Technical Medical Center, University of Twente, Enschede, The Netherlands
[2] Clinical Neurophysiology Group, Techmed Centre, University of Twente, Enschede, The Netherlands
[3] Department of Neurosurgery, Medisch Spectrum Twente, Enschede, The Netherlands

Abstract. Chronic subdural hematoma (cSDH) is a common neurological condition characterized by the accumulation of blood between the brain and the dura mater. This accumulation of blood can exert pressure on the brain, potentially leading to fatal outcomes. Treatment options for cSDH are limited to invasive surgery or non-invasive management. Traditionally, the midline shift, hand-measured by experts from an ideal sagittal plane, and the hematoma volume have been the primary metrics for quantifying and analyzing cSDH. However, these approaches do not quantify the local 3D brain deformation caused by cSDH. We propose a novel method using anatomy-aware unsupervised diffeomorphic pseudo-healthy synthesis to generate brain deformation fields. The deformation fields derived from this process are utilized to extract biomarkers that quantify the shift in the brain due to cSDH. We use CT scans of 121 patients for training and validation of our method and find that our metrics allow the identification of patients who require surgery. Our results indicate that automatically obtained brain deformation fields might contain prognostic value for personalized cSDH treatment. Our implementation is available on: `github.com/Barisimre/brain-morphing`

Keywords: Chronic subdural hematoma · Diffeomorphic Image Registration · Biomarker Extraction · Unsupervised Learning · Pseudo-Healthy Brain Synthesis.

1 Introduction

With an aging population, chronic subdural hematoma (cSDH) is an increasingly common neurological condition. cSDH is characterized by blood accumulation between the brain and dura mater that can pressure the brain, deform it, and potentially be fatal [1]. CT visualizes hematomas well (Fig. 1) and remains the most commonly used diagnostic tool for cSDH. However, currently, there is no consensus on cSDH treatment following CT imaging [2]. Treatment varies between
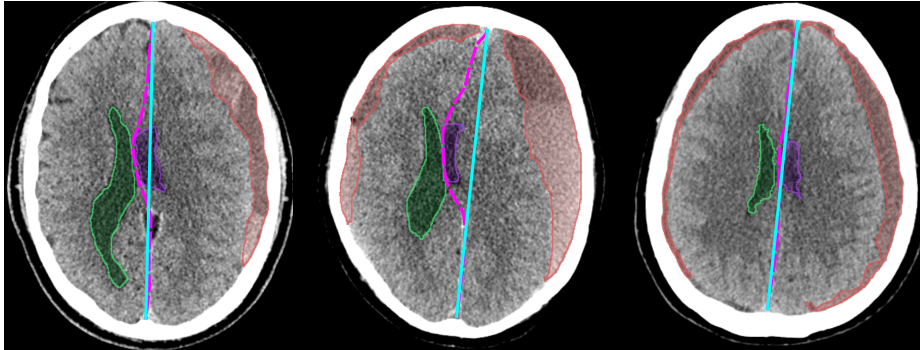
Fig. 1. CT scans of cSDH patients selected for surgical intervention, showing the ideal midline (blue), shifted midline (pink), cSDH (red), left ventricle (purple), and right ventricle (green). Left: a unilateral hematoma with midline shift. Center: a bilateral hematoma with midline shift. Right: a bilateral hematoma without midline shift.

wait-and-scan management and surgery [3]. Medical or endovascular treatments are subject to large trials [4].

Clinical decision-making could be improved with objective metrics to quantify the severity of cSDH. Currently, cSDH severity is quantified using geometric properties such as the midline or midplane shift of the brain and the volume of the hematoma [5, 6]. Various methods have studied automatic determination of midline shift [7–10] and midplane shift [11], and recent works have shown that the hematoma can be automatically segmented using deep learning [12]. However, these methods are global and fail to take the local effects of cSDH into account. Moreover, in the case of symmetric (bilateral) cSDH, midline shift might be minimal, while cSDH severity is significant (Fig. 1).

In this paper, we introduce a novel approach to quantitatively assess the severity of cSDH, by estimating the brain shift caused by the hematoma. We estimate this deformation using an unsupervised deep learning-based diffeomorphic method [13, 14]. Unlike common image registration problems, we do not have paired images for training our model since pre-disease brain scans are unavailable for most patients. Instead, we regularize our deformation model with personalized geometric priors to obtain a pseudo-healthy, symmetric brain. All geometric priors, i.e., the ideal midplane of the brain, 3D segmentation of hematomas and brain ventricles, and brain masks, are automatically obtained. We demonstrate that the diffeomorphic deformation fields generated by our methodology, and biomarkers extracted from these deformation fields, offer an accurate assessment of cSDH severity that complements traditional midline shift metrics.

2   Materials and Methods

Figure 2 outlines our method. Given a CT scan of a brain with cSDH, we automatically align the brain with canonical axes. Then, a Swin UNETR [15] model
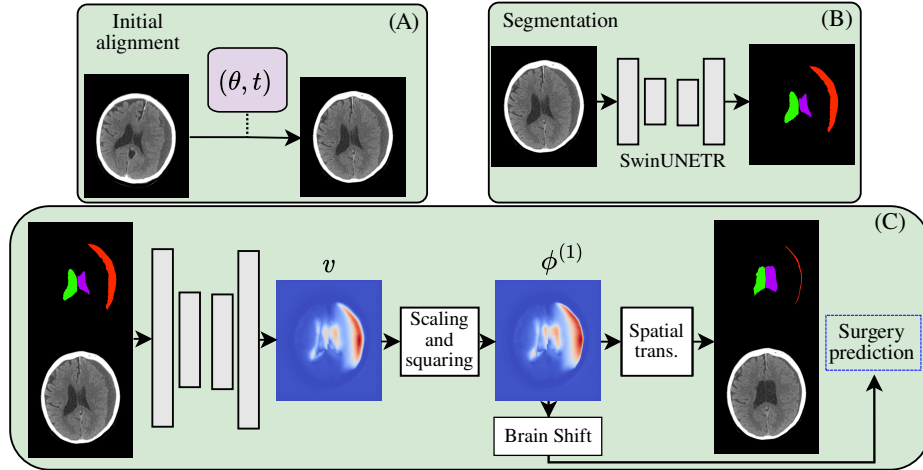
Fig. 2. Overview of our process. Images are aligned to a sagittal plane (A) and automatically segmented (B). The CT scan and segmentations are used as input to a deep diffeomorphic registration model (C). Deformation fields provided by this model are used to distinguish between patients requiring surgery by various biomarkers.

automatically segments the hematomas and ventricles. Images and segmentation masks are jointly used in an unsupervised diffeomorphic VoxelMorph-based [14] model that provides local velocity fields required to virtually remove the hematoma and translate the brain into its pseudo-healthy version.

2.1   Data

We used a retrospectively collected dataset of 121 patients scanned at Medisch Spectrum Twente between 2011 and 2019. A waiver from the local medical ethics committee was obtained. We excluded all scans that showed cSDH after a first surgical intervention. Selected scans had an in-plane resolution of $0.41 \pm 0.065 \times 0.40 \pm 0.070$ mm and a slice thickness of 3.42 ± 0.64 mm. All scans were resampled to a spatial resolution of $0.40 \times 0.40 \times 1.50$ mm. For the majority of patients, we know whether - based on the CT scan and other parameters - surgery was performed to mitigate the effects of cSDH. In total, 46 patients received surgery, and 68 did not. Seven patients without surgical status were excluded from the dataset. Surgical status serves as the endpoint for our prediction model. In a subset of 25 scans, the hematoma, left ventricle, and right ventricle were manually annotated in 3D using the XNAT OHIF viewer [16]. Annotations were made by technical physicians in training, and verified by a neurologist to ensure the quality and accuracy of the annotations. Moreover, manual measurements were obtained of the midline shift of each subject within the dataset.

2.2   Brain Symmetry Losses

In the initial alignment and diffeomorphic registration steps of our algorithm ((A) and (C) in Fig. 2), we use two fully differentiable losses that quantify brain symmetry. We initially split each volume $X \in \mathbb{R}^3$ into two equally sized volumes (X_{left} and X_{right}) by the mid-sagittal plane, halving the scan perfectly into two. Both of the losses use these pseudo-hemispheres as input. The two losses are the SSIM loss, derived as the negative of the structural symmetry index (SSIM), [17] $\mathcal{L}_{SSIM}$ and Jeffreys divergence loss $\mathcal{L}_{jeffrey}$ [18]. Let $H : \mathbb{R}^3 \to \mathbb{R}^1$ be the differentiable histogram function with n bins, introduced by Ustinova et al. [19]. The Jeffreys divergence loss $\mathcal{L}_{jeffrey}$ is calculated as the following, using histograms as probability distribution function surrogates:

$$\mathcal{L}_{jeffrey} = \sum_n H_n(X_{left}) \log \frac{H_n(X_{left})}{H_n(X_{right})} + \sum_n H_n(X_{right}) \log \frac{H_n(X_{right})}{H_n(X_{left})} \quad (1)$$

A higher value for $\mathcal{L}_{jeffrey}$ indicates that the two pseudo-hemispheres being compared have different intensity distributions, either due to a misalignment from the mid sagittal plane or the presence of a hematoma, contributing to a collection of many similar voxels grouped in intensity.

2.3   Initial Alignment and Segmentation

We rigidly align 3D volumes to establish a symmetry axis on the sagittal plane (the ideal midplane or mid-sagittal plane). In other words, we want the brains to be as symmetric as possible with respect to the center (mid) sagittal plane. We use iterative optimization with Adam [20]. At each step, we calculate the combined symmetry loss explained in Section 2.2 together with a volume loss term. We optimize four variables per scan, corresponding to the pitch, yaw, roll (θ), and translation (t) of the 3D volume, similarly to the process described by Prima et. al [21]. The volume loss ensures that both of the halves in the results have equal volumes of foreground, counting the total volume in both halves, using a differentiable binary operator $B : \mathbb{R}^3 \to \mathbb{R}^3$ that maps any non zero items to one and every zero items to zero. We find this volume loss especially useful in cases where the head is located far from the center of the scan.

$$\mathcal{L}_{volume} = \frac{|\sum B(X_{left}) - \sum B(X_{right})|}{\sum B(X)} \quad (2)$$

We segment the subdural hematomas, left ventricles, and ventricles in aligned 3D CT scans using a Swin UNETR [15] trained on manual segmentations. During training, we augment our data using random rotations, random 3D crops, and sagittal flips. We denote the result of segmenting image X as $S(X)$ below, with each segmentation class denoted as S_{class}.

2.4   Diffeomorphic Pseudo-Healthy Synthesis

For any brain with cSDH, we predict the deformation required to translate it into a pseudo-healthy equivalent. We train an image-to-image model that, given input volumes and masks, estimates a velocity field v that can be integrated over $t = [0, 1]$ using scaling and squaring [22] to obtain a deformation field $\phi^{(1)}$. This field is applied to the CT scan to obtain the pseudo-healthy brain $\phi(X)$.

We minimize a compound loss term, based on the pseudo-healthy brain $\phi(X)$, the deformation field $(\phi^{(1)})$, and the deformed segmentation masks $(\phi(S(X)))$. We aim to maximize the internal symmetry of the pseudo-healthy brains with the loss terms explained in Section 2.2. We separately apply the deformation to the segmentation masks $(S_{left}(X), S_{right}(X)$, and $S_{hematoma}(X))$ and calculate two loss terms. We maximize the symmetry of the ventricles by optimizing for their overlap when one of them is reflected on the sagittal plane using a Dice loss (Eq. 3). We target the removal of the hematomas by optimizing to reduce the volume in the deformed hematoma mask formalized with Eq. 4.

$$\mathcal{L}_{ventricle} = Dice(\phi(S_{left}(X)),\ SagittalFlip(\phi(S_{right}(X)))) \qquad (3)$$

$$\mathcal{L}_{hematoma} = 1 - \frac{\sum S_{hematoma}(X) - \sum \phi(S_{hematoma}(X))}{\sum S_{hematoma}(X)} \qquad (4)$$

We ensure the preservation of the skull with $\mathcal{L}_{skull}$, using the Dice loss of the original and deformed skull. We regularize the registration methods by introducing two additional loss terms. Firstly, we limit the shrinkage of non-hematoma voxels by a Jacobian regularizer. The Jacobian determinant $\det\nabla\Phi$ at any location indicates the expansion or shrinkage. We aim to regularize the Jacobian of the non-hematoma voxel to 1 and the hematoma voxels to 0. Secondly, we approximate the spatial gradient differences of the velocity field with the same method as Balakrishnan et. al. [23], shifting in all three dimensions by one and subtracting the velocity magnitudes. We find that applying this loss to the velocity field v rather than the deformation field $\phi^{(1)}$ produces smoother results. The deformation loss $\mathcal{L}_{deformation}$ is defined in Eq. 5.

$$\begin{aligned}\mathcal{L}_{deformation} =\ & \lambda_1\ \mathcal{L}_{jeffrey} + \lambda_2\ \mathcal{L}_{ssim} + \lambda_3\ \mathcal{L}_{ventricle} + \lambda_4\ \mathcal{L}_{hematoma} \\ & + \lambda_5\ \mathcal{L}_{skull} + \lambda_6\ \mathcal{L}_{jacobian} + \lambda_7\ \mathcal{L}_{gradient}\end{aligned} \qquad (5)$$

2.5   cSDH Severity Prediction

We use the deformation fields generated per scan to calculate three novel biomarkers of brain deformation, namely, the maximum, average, and sum of the magnitudes of voxel-wise deformation vectors (in mm). We divide the markers into two categories, conventional markers including hematoma volume and midline shift, and our three novel biomarkers. We fit a logistic regression classifier for each biomarker, in each data subset, with surgical outcome as target. We evaluate
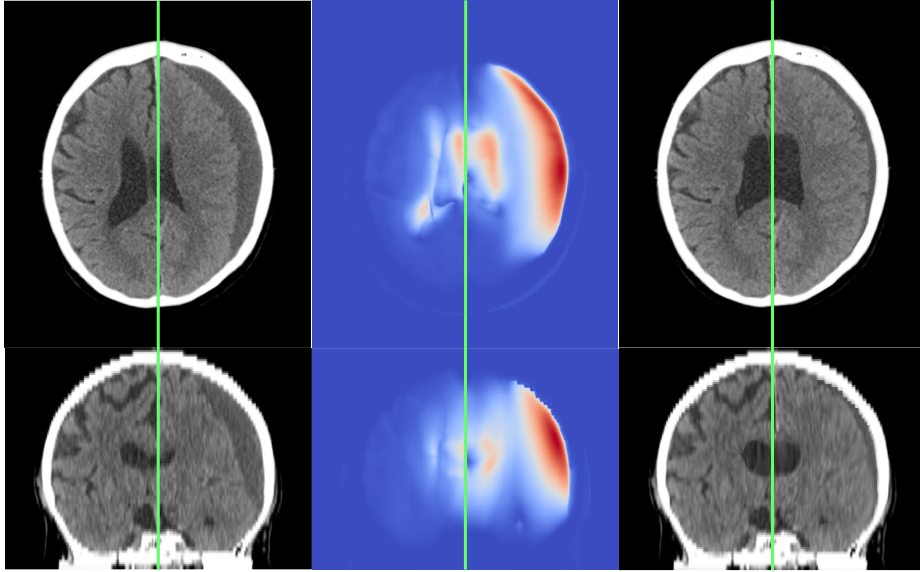
Fig. 3. Axial and coronal slide visualizing registration results and mid-sagittal plane (green). From left to right: the original brain with a unilateral (visible on the right side) cSDH, the magnitude of the deformation field, and the resulting pseudo-healthy brain. The hematoma is mostly removed and ventricular symmetry is restored.

the model's performance in the identification of patients requiring surgery using ROC curves. Moreover, we utilize TPOT [24] to identify the best-performing model for prediction based on combinations of these derived markers.

3   Experiments and Results

All experiments were conducted on a single machine with 128 GBs of RAM and an NVIDIA L40 GPU (48 GBs VRAM). Methods were implemented in PyTorch [25], and code is provided on GitHub[4]. We perform a five-fold cross-validation of the full model.

3.1   Initial Alignment and Segmentation

We observed that 150 iterations with a learning rate of 0.03 and Adam optimizer [20] was sufficient for initial image alignment. The Swin UNETR model is trained for 5000 epochs using the Adam optimizer and a learning rate of 3e-4. We observed an average Dice score of 0.82 for hematomas and 0.86 for both of the ventricles.

[4] github.com/Barisimre/brain-morphing
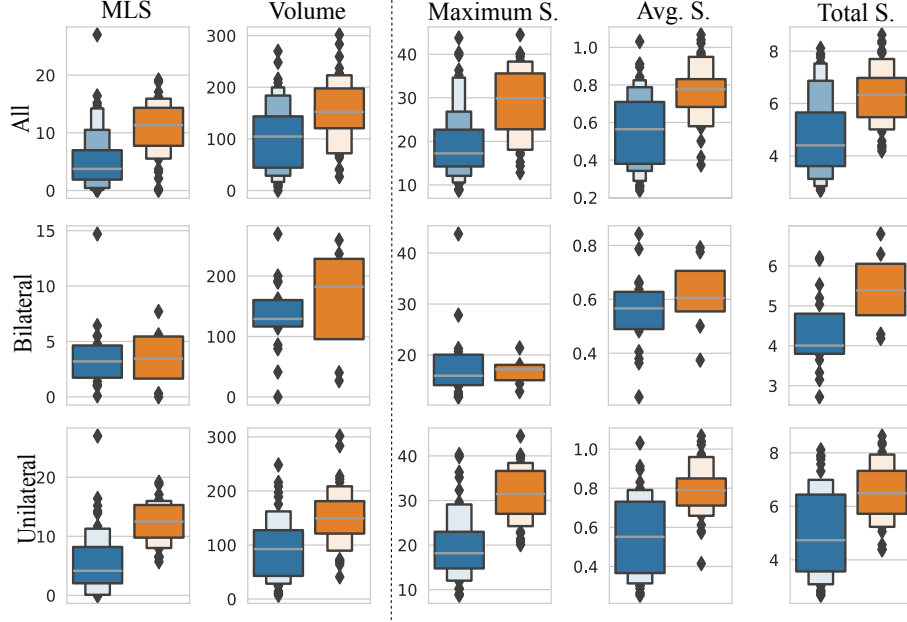
Fig. 4. Box plots for five biomarkers for three subsets of our data, comparing the distributions of patients that required surgery (orange) compared to the rest (blue). The midline shift (MLS) is hand measured in mm. Hematoma volume (Volume) is inferred from the segmentation results in mm. Maximum, average, and total shift are calculated as explained in subsection 2.5 in millimeters. Many of the biomarkers fail at distinguishing surgical status of bilateral hematomas.

3.2 Pseudo-Healthy Synthesis

For the pseudo-healthy synthesis process, we used the Adam optimizer with a learning rate of 3e-4. We trained this model for 20,000 iterations. Loss coefficients in Eq. 5 were chosen as 5.0 for $\mathcal{L}_{jacobian}$, $\mathcal{L}_{gradient}$, and $\mathcal{L}_{skull}$ and 1.0 for the rest. Figure 3 shows a qualitative example where the brain was clearly deformed in the hematoma area as well as on the contralateral side. Across all images, we observed an average hematoma volume reduction of 73 percent with a standard deviation of 13 percent. This indicates that the method is not able to remove all hematoma. In general, we found thin hematomas circling the brain around more difficult to reduce due to the regularization of the deformation fields.

3.3 Surgery Prediction

We investigated the distribution of five biomarkers in the group of patients that did not require surgery and the group that did. These biomarkers are the midline shift, hematoma volume, and our three markers derived from the deformation
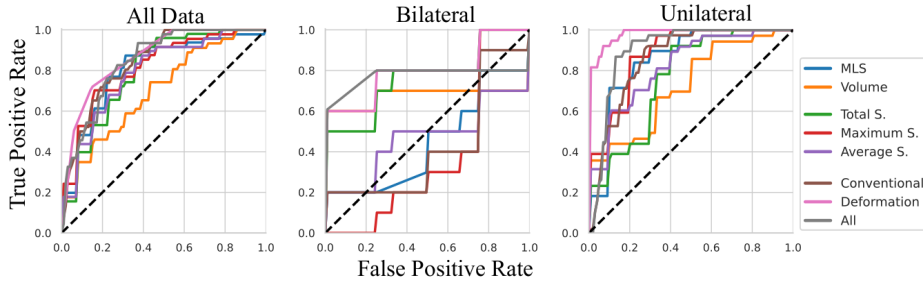
Fig. 5. ROC curves of surgical status classifiers in either the full population (left) or subgroups of patients with bilateral (center) or unilateral (right) hematomas.

Table 1. AUC scores of all classification models. MLS = midline shift. We present models for individual conventional and deformation-based biomarkers and combinations of biomarkers.

	Conventional		Deformation-based			Joint		
	MLS	Volume	Average	Max	Sum	Convent.	Deform.	All
All Data	0.80	0.70	0.79	0.81	0.79	0.84	**0.87**	0.84
Bilateral	0.44	0.67	0.48	0.37	0.76	0.42	**0.79**	0.77
Unilateral	0.85	0.72	0.82	0.87	0.76	0.86	**0.96**	0.90

fields: maximum, average, and sum. We performed a subgroup analysis on patients with bilateral or unilateral hematomas. Figure 4 confirms our hypothesis that midline shift (MLS) poorly separates patients with bilateral cSDH. However, separating these cases is also difficult for our maximum shift feature.

The receiver operating characteristic curves (ROC) for each of the classification models is shown in Figure 5. For the bilateral subset, only the total shift and hematoma volume as single markers were able to perform better than random in classification. Table 1 shows the area under the curve (AUC) results corresponding to these ROCs. In each subset, we observed that a marker generated from the deformations fields performs better than traditional markers, while the combination of all deformation-based markers performed the overall best.

4 Discussion and Conclusion

We have presented a novel pseudo-healthy brain synthesis process, with applications in cSDH patients. We have shown that symmetry losses can be used to obtain visually plausible pseudo-healthy CT scans of patients, and deformation fields from which features can be extracted for personalized treatment prediction. Our results confirm the hypothesis that biomarkers are affected by the laterality of the cSDH, where most biomarkers underperform in bilateral cSDH.

This study shows that there is valuable information in 3D context for cSDH assessments. Moreover, our work highlights the value of machine learning for

cSDH and neurosurgery. First, we fully automatically segment cSDH and ventricles in 3D CT volumes. Second, we obtain deformation fields with a generalizable model. Third, we use machine learning models to identify patients in need of surgery. The deformation fields that we obtain are diffeomorphic, which means that they also represent the inverse process of cSDH formation. In future works, this could be used to synthesize data of cSDH patients from healthy brains, and further our understanding of cSDH formation.

Our study has limitations. First, ground truth labels for our outcome - surgery or not - are subjective and vary per clinician [26], especially given the current lack of objective criteria for this decision. In future work, we aim to use our novel biomarkers to predict objective outcomes and correlate with invasive measurements of pressure [27]. Second, our model is not end-to-end, and errors might accumulate along our pipeline. For example, imperfect alignment might affect the performance of the segmentation model, which in turn might lead to incorrect deformation fields. In future work, we will investigate the development of an end-to-end model for joint segmentation and registration. Moreover, a larger data set might allow the extraction of more informative biomarkers. It has been shown that deformation fields might contain valuable prognostic information [28]. Finally, our heuristic symmetry losses could be extended with data-driven perceptual losses that define what a healthy brain looks like [29].

In conclusion, our results indicate that automatically obtained brain deformation fields might contain prognostic value for personalized cSDH treatment.

References

1. Blaauw, J. *et al.* Presenting symptoms and functional outcome of chronic subdural hematoma patients. *Acta Neurologica Scandinavica* **145,** 38–46 (2022).
2. Mehta, V., Harward, S. C., Sankey, E. W., Nayar, G. & Codd, P. J. Evidence based diagnosis and management of chronic subdural hematoma: A review of the literature. *Journal of Clinical Neuroscience* **50,** 7–15. ISSN: 0967-5868 (Apr. 2018).
3. Feghali, J., Yang, W. & Huang, J. Updates in Chronic Subdural Hematoma: Epidemiology, Etiology, Pathogenesis, Treatment, and Outcome. *World Neurosurgery* **141,** 339–345. ISSN: 1878-8750 (Sept. 2020).
4. Miah, I. P. *et al.* Dexamethasone versus Surgery for Chronic Subdural Hematoma. *New England Journal of Medicine* **388,** 2230–2240. ISSN: 1533-4406 (June 2023).
5. Miah, I. P. *et al.* Radiological prognostic factors of chronic subdural hematoma recurrence: a systematic review and meta-analysis. *Neuroradiology* **63,** 27–40. ISSN: 1432-1920 (Oct. 2020).

6. Zanolini, U. *et al.* Midline Shift in Chronic Subdural Hematoma: Interrater Reliability of Different Measuring Methods and Implications for Standardized Rating in Embolization Trials. *Clinical Neuroradiology* **32,** 931–938.

7. Liao, C.-C., Chen, Y.-F. & Xiao, F. Brain Midline Shift Measurement and Its Automation: A Review of Techniques and Algorithms. *International Journal of Biomedical Imaging* **2018,** 1–13. ISSN: 1687-4196 (2018).

8. Xiao, F., Liao, C.-C., Huang, K.-C., Chiang, I.-J. & Wong, J.-M. Automated assessment of midline shift in head injury patients. *Clinical Neurology and Neurosurgery* **112,** 785–790. ISSN: 0303-8467 (Nov. 2010).

9. Nag, M. K. *et al.* Quantitative analysis of brain herniation from non-contrast CT images using deep learning. *Journal of Neuroscience Methods* **349,** 109033.

10. Liu, R. *et al. From hemorrhage to midline shift: A new method of tracing the deformed midline in traumatic brain injury ct images* in *2009 16th IEEE International Conference on Image Processing (ICIP)* (Nov. 2009).

11. Xia, X. *et al.* Automated detection of 3D midline shift in spontaneous supratentorial intracerebral haemorrhage with non-contrast computed tomography using deep convolutional neural networks. *American Journal of Translational Research* **13,** 11513 (2021).

12. Kellogg, R. T. *et al.* Segmentation of Chronic Subdural Hematomas Using 3D Convolutional Neural Networks. *World Neurosurgery* **148,** e58–e65. ISSN: 1878-8750 (Apr. 2021).

13. Ashburner, J. A fast diffeomorphic image registration algorithm. en. *NeuroImage* **38,** 95–113 (2007).

14. Dalca, A. V., Balakrishnan, G., Guttag, J. & Sabuncu, M. R. Unsupervised learning of probabilistic diffeomorphic registration for images and surfaces. *Medical Image Analysis* **57,** 226–236 (Oct. 2019).

15. Hatamizadeh, A. *et al. Swin UNETR: Swin Transformers for Semantic Segmentation of Brain Tumors in MRI Images* 2022. arXiv: 2201.01266 [eess.IV].

16. Doran, S. J. *et al.* Integrating the OHIF Viewer into XNAT: Achievements, Challenges and Prospects for Quantitative Imaging Studies. *Tomography* **8,** 497–512 (2022).

17. Wang, Z., Bovik, A., Sheikh, H. & Simoncelli, E. Image quality assessment: from error visibility to structural similarity. *IEEE Transactions on Image Processing* **13,** 600–612 (2004).

18. Jeffreys, H. *The theory of probability* 3rd ed. en (Oxford University Press, London, England, July 1998).

19. Ustinova, E. & Lempitsky, V. *Learning Deep Embeddings with Histogram Loss* in *Advances in Neural Information Processing Systems* (eds Lee, D., Sugiyama, M., Luxburg, U., Guyon, I. & Garnett, R.) **29** (Curran Associates, Inc., 2016).

20. Kingma, D. P. & Ba, J. Adam: A method for stochastic optimization. *arXiv preprint arXiv:1412.6980* (2014).

21. Prima, S., Ourselin, S. & Ayache, N. Computation of the mid-sagittal plane in 3-D brain images. *IEEE Transactions on Medical Imaging* **21,** 122–138. ISSN: 0278-0062 (2002).

22. Arsigny, V., Commowick, O., Pennec, X. & Ayache, N. in *Lecture Notes in Computer Science* 924–931 (Springer Berlin Heidelberg, 2006).

23. Balakrishnan, G., Zhao, A., Sabuncu, M. R., Guttag, J. & Dalca, A. V. VoxelMorph: A Learning Framework for Deformable Medical Image Registration. *IEEE Transactions on Medical Imaging* **38,** 1788–1800. ISSN: 1558-254X (Aug. 2019).

24. Olson, R. S., Bartley, N., Urbanowicz, R. J. & Moore, J. H. *Evaluation of a Tree-based Pipeline Optimization Tool for Automating Data Science* in *Proceedings of the Genetic and Evolutionary Computation Conference 2016* (2016), 485–492. ISBN: 978-1-4503-4206-3.

25. Paszke, A. *et al.* in *Advances in Neural Information Processing Systems 32* 8024–8035 (2019).

26. Baschera, D., Tosic, L., Westermann, L., Oberle, J. & Alfieri, A. Treatment Standards for Chronic Subdural Hematoma: Results from a Survey in Austrian, German, and Swiss Neurosurgical Units. *World Neurosurgery* **116,** e983–e995. ISSN: 1878-8750 (Aug. 2018).

27. Sundstrøm, T., Helland, C. A., Aarhus, M. & Wester, K. What is the Pressure in Chronic Subdural Hematomas? A Prospective, Population-Based Study. *Journal of Neurotrauma* **29.** PMID: 21635185, 137–142 (2012).

28. Trebeschi, S. *et al.* Development of a prognostic AI-monitor for metastatic urothelial cancer patients receiving immunotherapy. *Frontiers in Oncology* **11,** 637804 (2021).

29. Baumgartner, C. F., Koch, L. M., Tezcan, K. C., Ang, J. X. & Konukoglu, E. *Visual feature attribution using wasserstein gans* in *Proceedings of the IEEE conference on CVPR* (2018), 8309–8319.